Journal of the Korean Ceramic Society
Vol. 53, No. 3, pp. 306~311, 2016.

http://dx.doi.org/10.4191/kcers.2016.53.3.306

Investigation of LiO_2 Adsorption on $LaB_{1-x}B'_xO_3$(001) for Li-Air Battery Applications: A Density Functional Theory Study

Hyunguk Kwon and Jeong Woo Han†

Department of Chemical Engineering, University of Seoul, Seoul 02504, Korea

(Received April 12, 2016; Revised April 26, 2016; Accepted April 27, 2016)

ABSTRACT

Li-air batteries have received much attention due to their superior theoretical energy density. However, their sluggish kinetics on the cathode side is considered the main barrier to high performance. The rational design of electrode catalysts with high activity is therefore an important challenge. To solve this issue, we performed density functional theory (DFT) calculations to analyze the adsorption behavior of the LiO_2 molecule, which is considered to be a key intermediate in both the Li-oxygen reduction reaction (ORR) and the evolution reaction (OER). Specifically, to use the activity descriptor approach, the LiO_2 adsorption energy, which has previously been demonstrated to be a reliable descriptor of the cathode reaction in Li-air batteries, was calculated on $LaB_{1-x}B'_xO_3$(001) (B, B' = Mn, Fe, Co, and Ni, x = 0.0, 0.5). Our fast screening results showed that $LaMnO_3$, $LaMn_{0.5}Fe_{0.5}O_3$, or $LaFeO_3$ would be good candidate catalysts. We believe that our results will provide a way to more efficiently develop new cathode materials for Li-air batteries.

Key words : Li-air battery cathode, $LaBO_3$ perovskite, LiO_2 adsorption, Density functional theory

1. Introduction

The use of fossil fuels has exacerbated various environmental concerns, particularly global warming. To reduce the dependence on fossil fuels, nowadays Li-air batteries, due to their high theoretical specific energy, have attracted interest for future electric vehicles, electrical energy storage devices, and other energy applications.[1-3] However, many scientific issues such as low round-trip efficiency, short cycle life, poor rate capability, and electrolyte instability must be solved for the realization of affordable Li-air battery technology.[4-9] Especially, the slow kinetic rate of the oxygen reduction reaction (ORR) or the oxygen evolution reaction (OER) on the cathode side has been widely known as a main obstacle to high energy efficiency.[10] To overcome this problem, numerous attempts have been made to design new electrocatalysts with high activity for ORR or OER.[11] In the past, perovskite oxides (ABO_3) have been nominated as potential ORR or OER catalysts[12,13] due to their high catalytic activity, fast electronic and ionic conductivity, and low cost.[12,14,15] For these reasons, many researchers have made efforts to enhance the cathode kinetics using $LaBO_3$-type perovskite oxides such as $LaSrMnO_3$,[16,17] $LaFeO_3$,[18] and $LaSrCoO_{3-\delta}$[19] in Li-air batteries. However, in spite of these constant efforts, it is still difficult to find optimal combinations of components in perovskite oxides due to changes in catalytic properties with partial or full substitution at A- and B-sites.

Previous studies have provided efficient ways to improve the catalytic properties. Introducing an activity descriptor enables us to facilitate fast screening of perovskite catalysts for Li-air batteries.[14,15] Using density functional theory (DFT) calculations, Nørskov *et al.*[20] suggested a method that can assess the thermochemistry of the electrochemical reactions. They also verified the origin of the overpotential for oxygen reduction over Pt(111). Based on these results, Man *et al.*[21] derived a descriptor (ΔG_{O^*}–ΔG_{HO^*}) for oxygen reduction using different kinds of oxide materials. These results has been widely applied in various electrochemical reactions including Li-ORR and OER to introduce useful descriptors. Choi *et al.*[22] used the DFT calculated adsorption energy database of lithium oxide intermediates to examine the theoretical overpotentials for ORR and OER on Pd, Cu, and PdCu alloy surfaces with an ordered body centered cubic (B2-type) structure. They reported that the LiO_2 adsorption energy shows a good correlation with the ORR and/or OER overpotentials. Moreover, they demonstrated that controlling the LiO_2 adsorption energy by alloying the material with Pd and Cu can enhance the catalytic activity. A similar argument was also made by Kim *et al.,*[23] who suggested that the overpotential of Li-OER decreases with decreasing of the strength of LiO_2 adsorption on Pt(111), Co(0001), and Pt_3Co(111). These results motivated us to estimate the catalytic activity on perovskite oxides by using only a simple descriptor, the LiO_2 adsorption energy.

In this study, we first use DFT calculations to perform a structural investigation of the LiO_2 adsorption on LaB_{1-}

†Corresponding author : Jeong Woo Han
E-mail : jwhan@uos.ac.kr
Tel : +82-2-6490-2373 Fax : +82-2-6490-2364

$_xB'_xO_3$(001) (B, B' = Mn, Fe, Co, and Ni, x = 0.0, 0.5). Then, charge analysis of the adsorption behavior is performed to understand the phenomenon in detail. Finally, the energetics of LiO_2 adsorption is investigated to rapidly predict promising candidate perovskite catalysts. In order to tune the adsorption energy, which is closely related to the catalytic activity, we dope the B-site metal site with other 3*d*-transition metal species.[24-26]

2. Computational Methods

All periodic density functional theory (DFT) calculations were performed using the Vienna *Ab initio* Simulation Package (VASP).[27,28] The Perdew-Burke-Ernzerhof (PBE) functional, based on the generalized gradient approximation (GGA), was employed.[29] In addition, the DFT+U method[30] with U_{eff} = 4.0 eV (Mn), 4.0 eV (Fe), 3.3 eV (Co), and 6.4 eV (Ni)[31] was applied to reduce the self-interaction error. All calculations included spin polarization and were performed with a cutoff of 400 eV. Geometries were optimized until the forces on each atom were below 0.03 eV $Å^{-1}$. The optimized lattice constants were obtained using 2 × 2 × 2 supercells. An asymmetric slab structure was constructed by cleaving the bulk structure along the (001) plane. For the calculations of (2 × 2) surface unit cells with 4 atomic layers, an 8 × 8 × 1 Monkhorst-Pack[32] grid *k*-point mesh was used. The slab models have two fixed bottom layers as the bulk positions and two fully relaxed top layers. A 15 Å vacuum layer was used to prevent interaction between the two periodic slabs. In all surface calculations, a dipole correction was applied in the perpendicular direction.[33] We used BO_2-terminated (001) surfaces, which often show high catalytic activity due to B-site metals.[14,15] Fig. 1 shows the bare and doped perovskite surface structures used in this study.

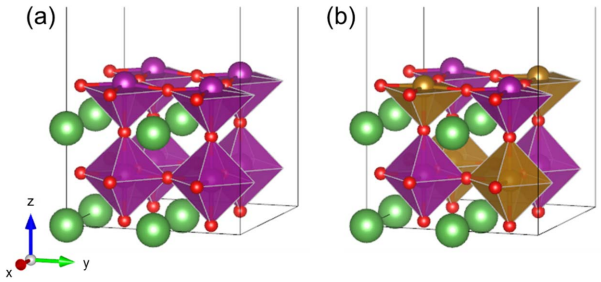

Fig. 1. Unit cell of (a) $LaBO_3$ and (b) $LaB_{50}B'_{50}O_3$ perovskite surfaces. La (lanthanum) atoms are green spheres, B or B' (transition metal) atoms are purple or brown spheres, and O (oxygen) atoms are red spheres.

The adsorption energy of LiO_2 was calculated by

$$E_{ads}^{LiO_2}(eV) = E_{LiO_2/surf} - E_{LiO_2(g)} - E_{surf} \quad (1)$$

where $E_{ads}^{LiO_2}$ is the adsorption energy of LiO_2 on the perovskite surfaces. $E_{LiO_2/surf}$, $E_{LiO_2(g)}$, and E_{surf} are the total energies of surfaces with adsorbed LiO_2, an LiO_2 molecule in the gas phase, and the bare surface, respectively.[34] For the calculations of LiO_2 in the gas phase, a large periodically repeating cubic box, approximately 10 Å on a side, was used as a unit cell. Table 1 indicates the geometric information of the optimized LiO_2 molecule, which shows good agreement with previous experimental measurements.[35]

Quantitative charge transfer analysis between adsorbates and surfaces allows us to deeply understand the adsorption phenomenon. Thus, an electron density analysis using the Bader charge model[36,37] was carried out. A 12 × 12 × 1 Monkhorst-Pack[32] grid *k*-point mesh was used for the Bader charge analysis.

3. Results and Discussion

3.1 LiO_2 adsorption on $LaBO_3$(001)

We first examined the adsorption phenomenon of LiO_2 molecules on undoped perovskite ($LaBO_3$) surfaces because these surfaces have relatively simple structures. Dathar *et al.* previously reported that the first e^- transfer step of Li-ORR on a metal surface can be divided into associative and dissociative mechanisms depending on the activation barrier (E_a) for dissociating oxygen molecules.[38] They suggested that a Li atom reacts with an oxygen molecule on metal surfaces with high E_a (LiO_2 generation), whereas it reacts with dissociated oxygen atoms on surfaces with low E_a (OLiO generation). Unlike the case of metal surfaces, the initial adsorption mechanism on $LaBO_3$-type perovskite surfaces is still unclear. However, the O_2 dissociation reaction often shows a high activation barrier (~ 1 eV) on A-site undoped $LaBO_3$-type perovskites,[39,40] which would have few oxygen vacancies due to the good balance of charge. This means that the first e^- transfer step of Li-ORR on $LaBO_3$ perovskite surfaces may be associative adsorption. Hence, we here examined the adsorption energies and site preferences of the LiO_2 molecule, not the OLiO molecule.

Figure 2 shows the DFT-optimized LiO_2 adsorbed $LaMnO_3$ surface structure as a representative case. The O_2 part in LiO_2 is adsorbed on the top layer Mn atom. This is similar to previous reports in which the adsorption site of an O_2 molecule on an ABO_3 perovskite surface is the B-transition metal site.[39-42] The Li atom in LiO_2 is adsorbed on the 4-fold site surrounded by four lattice oxygen atoms. This

Table 1. Comparison between Calculated and Measured LiO_2 Geometric Information

	Symmetry	d(O–O) (Å)	d(Li–O) (Å)	< O–Li–O (°)
DFT (This work)	C_{2V}	1.367	1.782	45
Experiment[35] (Previous work)	C_{2V}	1.33±0.06	1.77±0.07	44

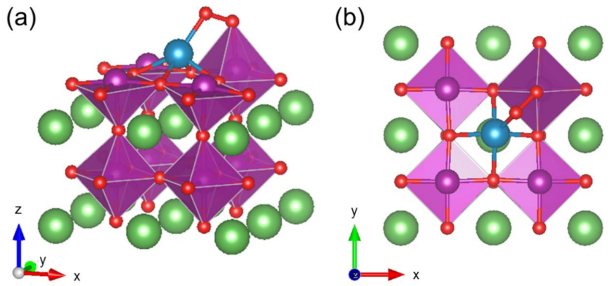

Fig. 2. (a) Side and (b) top views of LiO_2-adsorbed $LaMnO_3$ surface. La atoms are green spheres, Mn atoms are purple spheres, O atoms are red spheres, and Li atoms are blue-green spheres.

adsorption site preference of LiO_2 on the $LaMnO_3$ surface was almost identical for the other $LaBO_3$ perovskite surfaces examined in this study. However, the adsorption strength of LiO_2 shows clear differences. The trend in the adsorption energies on $LaBO_3$(001) (B = Mn, Fe, Co, and Ni) follows the order of atomic number of the B-transition metals in the periodic table (Table 2). This implies that the LiO_2 adsorption energy is mainly affected by the properties of transition metals in the B-site.

3.2 LiO_2 adsorption on $LaB_{0.5}B'_{0.5}O_3$(001)

Our results for the undoped perovskites in Section 3.1 provide useful insight into how we determined the binding site of LiO_2 on the B-site doped perovskite surfaces, $LaB_{0.5}B'_{0.5}O_3$(001). As can be seen in Fig. 1(b), there are two possible adsorption sites according to the two types of transition metals exposed on the surface (B and B'). Based on the results of adsorption on the undoped $LaBO_3$(001), we can reasonably assume that the O_2 part of LiO_2 is adsorbed on the top of B or B' cations, while the Li atom in LiO_2 binds only on the 4-fold site surrounded by four lattice oxygen atoms. We thus calculated the adsorption energies by considering those two possible adsorption sites for all $LaB_{0.5}B'_{0.5}O_3$(001) (Fig. 3 and Table 3).

It is found that the adsorption energy and site preference of LiO_2 on $LaB_{0.5}B'_{0.5}O_3$ surfaces are not dependent on those characteristics of the undoped $LaBO_3$ or $LaB'O_3$ surfaces. For example, the adsorption strength of LiO_2 (–2.05 eV) on the Co atom of $LaCoO_3$(001) is larger than that (-1.75 eV) on the Mn atom of $LaMnO_3$(001) (Because an Li atom is always absorbed at a site surrounded by four oxygen atoms, here we only mention the adsorption sites of the O_2 part in LiO_2). On the other hand, in $LaMn_{0.5}Co_{0.5}O_3$(001), the adsorption strength of LiO_2 (-2.21 eV) on the Mn atom is larger than that (-2.06 eV) on the Co atom. Furthermore, the adsorption strength on $LaMn_{0.5}Co_{0.5}O_3$(001) becomes much stronger than that on $LaMnO_3$(001) or $LaCoO_3$(001). These unpredictable tendencies of the site preferences and adsorption energies of LiO_2 imply that it is hard to minutely tune the adsorption energy (further, the activity) by doping

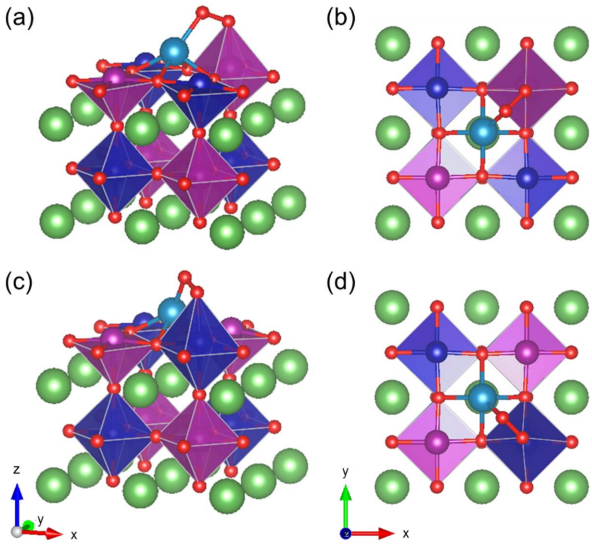

Fig. 3. LiO_2 adsorption on (a), (b) Mn atoms and (c), (d) Co atoms in $LaMn_{0.5}Co_{0.5}O_3$(001). (a), (c) indicate the side view while (c), (d) indicate the top view. La atoms are green spheres, Mn atoms are purple spheres, Co atoms are deep blue spheres, O atoms are red spheres, and Li atoms are blue-green spheres.

Table 2. Adsorption Energies of LiO_2 on $LaBO_3$(001) (B = Mn, Fe, Co, and Ni)

	$LaMnO_3$	$LaFeO_3$	$LaCoO_3$	$LaNiO_3$
E_{ads} of LiO_2 (eV)	–1.75	–1.87	–2.05	–2.61

Table 3. Adsorption Energies and Site Preferences of LiO_2 on $LaB_{0.5}B'_{0.5}O_3$(001) (B, B' = Mn, Fe, Co, and Ni). The B- and B'-sites Mean the Adsorption Sites of O_2 in LiO_2

$La(B_{0.50}B'_{0.50})O_3$	E_{ads} of LiO_2 (eV)		The most stable site
	B-site	B'-site	
$La(Mn_{0.50}Fe_{0.50})O_3$	–1.48	–1.84	Fe
$La(Mn_{0.50}Co_{0.50})O_3$	–2.21	–2.06	Mn
$La(Mn_{0.50}Ni_{0.50})O_3$	–2.26	–2.17	Mn
$La(Fe_{0.50}Co_{0.50})O_3$	–2.15	–2.51	Co
$La(Fe_{0.50}Ni_{0.50})O_3$	–2.18	–2.16	Fe
$La(Co_{0.50}Ni_{0.50})O_3$	–2.25	–2.26	Co or Ni

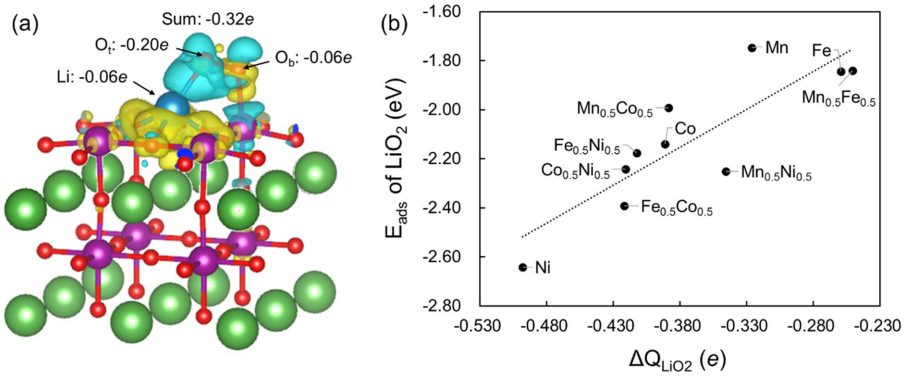

Fig. 4. (a) Changes in the electron density upon LiO_2 adsorption on $LaMnO_3$(001). Yellow and cyan colors indicate decreased and increased electron densities, respectively. O_t and O_b indicate the atomic oxygens located at the top and bottom of the adsorbed LiO_2 molecule, respectively. The isosurface contour is plotted with a charge density value of 0.002 e/Å^3. (b) Adsorption energies as a function of the charge density differences on the LiO_2 adsorbed $LaB_{1-x}B'_xO_3$(001) (B, B' = Mn, Fe, Co, and Ni, x = 0.0, 0.5). Each point indicates the pure or mixed B-site cations used in this system.

or mixing of different metals in perovskite oxides. As a result, determining the fundamental origin of the characteristic adsorption phenomena must be definitively resolved and is a subject for further study.

3.3 Charge density difference analysis

Adsorption is often accompanied by charge density redistribution. Thus, to understand the adsorption phenomenon in detail, we analyzed the charge density difference using Bader charge analysis.[36,37] Here, we demonstrate the results on $LaMnO_3$(001) as a representative case. Fig. 4(a) indicates that charges of -0.20e, -0.06e, and -0.06e transfer from the $LaMnO_3$ surface to the O_t, O_b, and Li in the LiO_2 molecule, respectively (Here, O_t, and O_b indicate the atomic oxygens located at the top and bottom, respectively, of the adsorbed LiO_2 molecule). Overall, -0.32e transfers from the surface to the adsorbate (LiO_2). This tendency was also observed in the other perovskite surfaces we examined in this study. O_t has the most negative charge state and O_b and Li have relatively lower negative charge states after adsorption. Moreover, the total charge density differences of adsorbed LiO_2 always have negative values; these values are related to the adsorption energies of LiO_2. Fig. 4(b) shows the adsorption energies as a function of the changes in electron density on the ten bare or doped perovskite surfaces. Overall, the adsorption strength increases with increasing transfer of electrons from the perovskite surface to the adsorbed LiO_2 molecule. These results indicate that the adsorption strength of the LiO_2 molecule is mainly determined by electron charge transfer between the adsorbate and the perovskite oxide surface.

3.4 Significance of LiO_2 adsorption analysis for Li-air battery cathodes

As mentioned earlier, LiO_2 adsorption energy can be a useful descriptor for the activity because the weak adsorption strength of LiO_2 is closely associated with the low overpotentials of ORR or OER.[22,23] To estimate the activity of electrocatalysts for Li-air batteries, we assessed the adsorption energies of LiO_2. Fig. 5 shows the DFT-calculated adsorption energies found in this study (reorganized from Tables 2 and 3). More red color means a weaker strength of LiO_2 adsorption, while more blue color indicates stronger strength. Our results suggest that among the lanthanum based perovskites $LaMnO_3$, $LaMn_{0.5}Fe_{0.5}O_3$, or $LaFeO_3$ would be good candidate materials as Li-air battery cathodes in terms of the reaction kinetics due to the weak adsorption strength of LiO_2. Indeed, some of these materials such as $LaSrMnO_3$ or $LaFeO_3$ have already shown high electrochemical performance in Li-air batteries.[16-18] This implies that our DFT results at the atomic scale provide a plausible explanation of the experimental results. To elucidate the detailed mechanism of ORR or OER in Li-air battery electrodes, a more thorough investigation for each elementary step will be required.

In addition, unlike the case on metal surfaces,[22,23,38,43] the adsorption phenomenon of Li-ORR or OER intermediates on perovskite surfaces have not been precisely determined at the atomic scale. Therefore, adsorption analysis of LiO_2, a key intermediate of Li-ORR or OER, on a wide range of per-

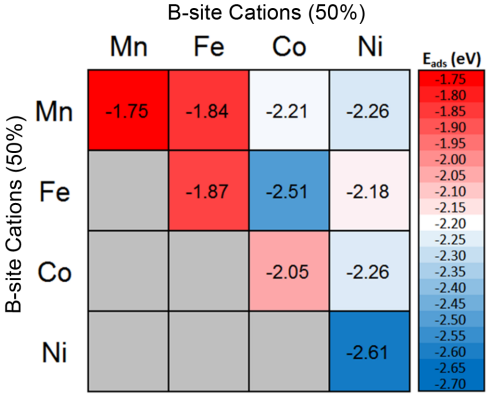

Fig. 5. Adsorption energies of LiO_2 on $LaB_{1-x}B'_xO_3$ (B, B' = Mn, Fe, Co, and Ni, x = 0.0, 0.5) perovskite surfaces.

ovskite surfaces may provide useful insight into the adsorption study of the other intermediates.

4. Conclusions

In this study, we carried out structural, charge, and energetic investigations of LiO_2 adsorption behaviors on $LaB_{1-x}B'_xO_3$(001) (B, B' = Mn, Fe, Co, and Ni, x = 0.0, 0.5) using DFT+U calculations. Unlike that of metal catalysts, the adsorption of lithium oxide intermediates on perovskite surfaces has hardly been examined. Our structural analysis showed that the adsorbed LiO_2 has a similar adsorption site preference and structure in all BO_2-terminated $LaB_{1-x}B'_xO_3$(001). Charge analysis demonstrated that the charge transfer from the perovskite surface to the LiO_2 molecule upon adsorption is a crucial factor for LiO_2 adsorption. LiO_2 adsorption energy was used as an activity descriptor to estimate the catalytic activities on $LaB_{1-x}B'_xO_3$(001). Our results showed that $LaMnO_3$, $LaMn_{0.5}Fe_{0.5}O_3$, or $LaFeO_3$ are promising candidate catalysts due to their weak LiO_2 adsorption, even though the cathode performance is dependent on a number of other factors. The screening results we present here also offer useful insight for experimental research into a rational design of perovskite catalysts for Li-air batteries.

Acknowledgments

The authors acknowledge financial support from the Basic Science Research Program (2014R1A1A1005303) and the Global Frontier R&D Program of the Center for Multiscale Energy Systesm (NRF-2014M3A6A7074785), through the National Research Foundation of Korea (NRF), funded by the Ministry of Science, ICT & Future Planning; they would also like to acknowledge supercomputing resources, including technical support, from the Supercomputing Center/Korea Institute of Science and Technology Information (KSC-2015-C3-045).

REFERENCES

1. P. G. Bruce, S. A. Freunberger, L. J. Hardwick, and J.-M. Tarascon, "Li–O_2 and Li–S Batteries with High Energy Storage," *Nat. Mater.,* **11** [1] 19-29 (2011).
2. R. Black, B. Adams, and L. F. Nazar, "Non-Aqueous and Hybrid Li-O_2 Batteries," *Adv. Energy Mater.,* **2** [7] 801-15 (2012).
3. J. Christensen, P. Albertus, R. S. Sanchez-Carrera, T. Lohmann, B. Kozinsky, R. Liedtke, J. Ahmed, and A. Kojic, "A Critical Review of Li/Air Batteries," *J. Electrochem. Soc.,* **159** [2] R1-30 (2012).
4. A. C. Luntz and B. D. McCloskey, "Nonaqueous Li–Air Batteries: A Status Report," *Chem. Rev.,* **114** [23] 11721-50 (2014).
5. Y. Lu, D. G. Kwabi, K. P. C. Yao, J. R. Harding, J. Zhou, L. Zuin, and Y. Shao-Horn, "The Discharge Rate Capability of Rechargeable Li-O_2 Batteries," *Energy Environ. Sci.,* **4** [8] 2999-3007 (2011).
6. S. S. Zhang, D. Foster, and J. Read, "Discharge Characteristic of A Non-Aqueous Electrolyte Li/O_2 Battery," *J. Power Sources,* **195** [4] 1235-40 (2010).
7. A. Debart, A. J. Paterson, J. Bao, and P. G. Bruce, "α-MnO_2 Nanowires: A Catalyst for the O_2 Electrode in Rechargeable Lithium Batteries," *Angew. Chemie Int. Ed.,* **47** [24] 4521-24 (2008).
8. A. Débart, J. Bao, G. Armstrong, and P. G. Bruce, "An O_2 Cathode for Rechargeable Lithium Batteries: The Effect of A Catalyst," *J. Power Sources,* **174** [2] 1177-11 (2007).
9. Z. Peng, S. A. Freunberger, Y. Chen, and P. G. Bruce, "Reversible and Higher-Rate Li-O_2 Battery," *Science,* **337** [6094] 563-66 (2012).
10. G. Girishkumar, B. McCloskey, A. C. Luntz, S. Swanson, and W. Wilcke, "Lithium-Air Battery: Promise and Challenges," *J. Phys. Chem. Lett.,* **1** [14] 2193-203 (2010).
11. Y. Shao, S. Park, J. Xiao, J.-G. Zhang, Y. Wang, and J. Liu, "Electrocatalysts for Nonaqueous Lithium–Air Batteries: Status, Challenges, and Perspective," *ACS Catal.,* **2** [5] 844-57 (2012).
12. D. B. Meadowcroft, "Low-Cost Oxygen Electrode Material," *Nature,* **226** [5248] 847-48 (1970).
13. J. O. Bockris and T. Otagawa, "The Electrocatalysis of Oxygen Evolution on Perovskites," *J. Electrochem. Soc.,* **131** [2] 290-302 (1984).
14. J. Suntivich, H. A. Gasteiger, N, Yabuuchi, H. Nakanishi, J. B. Goodenough, and Y. Shao-Horn, "Design Principles for Oxygen-Reduction Activity on Perovskite Oxide Catalysts for Fuel Cells and Metal–Air Batteries," *Nat. Chem.,* **3** [7] 546-50 (2011).
15. J. Suntivich, K. J. May, H. A. Gasteiger, J. B. Goodenough, and Y. Shao-Horn, "A Perovskite Oxide Optimized for Oxygen Evolution Catalysis from Molecular Orbital Principles," *Science,* **334** [6061] 1383-85 (2011).
16. J.-J. Xu, D. Xu, Z.-L. Wang, H.-G. Wang, L.-L. Zhang, and X.-B. Zhang, "Synthesis of Perovskite-Based Porous $La_{0.75}Sr_{0.25}MnO_3$ Nanotubes as A Highly Efficient Electrocatalyst for Rechargeable Lithium-Oxygen Batteries," *Angew. Chemie Int. Ed.,* **52** [14] 3887-90 (2013).
17. Z. Fu, X. Lin, T. Huang, and A. Yu, "Nano-Sized $La_{0.8}Sr_{0.2}MnO_3$ as Oxygen Reduction Catalyst in Nonaqueous Li/O_2 Batteries," *J. Solid State Electrochem.,* **16** [4] 1447-52 (2012).
18. J.-J. Xu, Z.-L. Wang, D. Xu, F.-Z. Meng, and X.-B. Zhang, "3D Ordered Macroporous $LaFeO_3$ as Efficient Electrocatalyst for Li-O_2 Batteries with Enhanced Rate Capability and Cyclic Performance," *Energy Environ. Sci.,* **7** [7] 2213-19 (2014).
19. Y. Zhao, L. Xu, L. Mai, C. Han, Q. An, X. Xu, X. Liu, and Q. Zhang, "Hierarchical Mesoporous Perovskite $La_{0.5}Sr_{0.5}CoO_{2.91}$ Nanowires with Ultrahigh Capacity for Li-Air Batteries," *Proc. Natl. Acad. Sci.,* **109** [48] 19569-74 (2012).
20. J. K. Nørskov, J. Rossmeisl, A. Logadottir, L. Lindqvist, J. R. Kitchin, and T. Bligaard, "Origin of the Overpotential for Oxygen Reduction at A Fuel-Cell Cathode," *J. Phys. Chem. B,* **108** [46] 17886-92 (2004).
21. I. C. Man, H. -Y. Su,. F. Calle-Vallejo, H. A. Hansen, J. I. Martínez, N. G. Inoglu, J. Kitchin, T. F. Jaramillo, and J. K. Nørskov, "Universality in Oxygen Evolution Electroca-

talysis on Oxide Surfaces," *ChemCatChem,* **3** [7] 1159-65 (2011).
22. R. Choi, J. Jung, G. Kim, K. Song, Y.-I. Kim, S. C. Jung, Y.-K. Han, H. Song, and Y.-M. Kang, "Ultra-Low Overpotential and High Rate Capability in Li-O_2 Batteries Through Surface Atom Arrangement of PdCu Nanocatalysts," *Energy Environ. Sci.*, **7** [4] 1362-68 (2014).
23. B. G. Kim, H.-J. Kim, S. Back, K. W. Nam, Y. Jung, Y.-K. Han, and J. W. Choi, "Improved Reversibility in Lithium-oxygen Battery: Understanding Elementary Reactions and Surface Charge Engineering of Metal Alloy Catalyst," *Sci. Rep.,* **4** 4225 (2014).
24. N. B. Halck, V. Petrykin, P. Krtil, and J. Rossmeisl, "Beyond the Volcano Limitations in Electrocatalysis - Oxygen Evolution Reaction," *Phys. Chem. Chem. Phys.*, **16** [27] 13682-88 (2014).
25. P. Liao, J. A. Keith, and E. A. Carter, "Water Oxidation on Pure and Doped Hematite (0001) Surfaces: Prediction of Co and Ni as Effective Dopants for Electrocatalysis," *J. Am. Chem. Soc.*, **134** [32] 13296-309 (2012).
26. Z. Xu and J. R. Kitchin, "Relationships between the Surface Electronic and Chemical Properties of Doped 4d and 5d Late Transition Metal Dioxides," *J. Chem. Phys.*, **142** [10] 104703-11 (2015).
27. G. Kresse and J. Furthmüller, "Efficient Iterative Schemes for Ab Initio Total-Energy Calculations Using a Plane-wave Basis Set," *Phys. Rev. B*, **54** [16] 11169-86 (1996)
28. G. Kresse and J. Furthmüller, "Efficiency of Ab-initio Total Energy Calculations for Metals and Semiconductors Using a Plane-wave Basis Set," *Comput. Mater. Sci.*, **6** [1] 15-50 (1996).
29. J. P. Perdew, K. Burke, and M. Ernzerhof, "Generalized Gradient Approximation Made Simple," *Phys. Rev. Lett.*, **77** [18] 3865-68 (1996).
30. S. L. Dudarev, G. A. Botton, S. Y. Savrasov, C. J. Humphreys, and A. P. Sutton, "Electron-Energy-Loss Spectra and the Structural Stability of Nickel Oxide: An LSDA+*U* Study," *Phys. Rev. B,* **57** [3] 1505-9 (1998).
31. L. Wang, T. Maxisch, and G. Ceder, "Oxidation Energies of Transition Metal Oxides within the GGA+*U* Framework," *Phys. Rev. B*, **73** [19] 195107 (2006).
32. H. J. Monkhorst and J. D. Pack, "Special Points for Brillouin-Zone Integrations," *Phys. Rev. B*, **13** [12] 5188-92 (1976).
33. G. Makov and M. Payne, "Periodic Boundary Conditions in *ab initio* Calculations," *Phys. Rev. B*, **51** [7] 4014-22 (1995).
34. D. S. Sholl and J. A. Steckel, Density Functional Theory: A Practical Introduction; pp. 94-97, John Wiley & Sons, Inc., Hoboken, New Jersey, 2009.
35. L. Andrews, "Infrared Spectrum, Structure, Vibrational Potential Function, and Bonding in the Lithium Superoxide Molecule LiO_2," *J. Chem. Phys.,* **50** [10] 4288-99 (1969).
36. R. F. W. Bader, "Atoms in Molecules," *Acc. Chem. Res.,* **18** [1] 9-15 (1985).
37. W. Tang, E. Sanville, and G. Henkelman, "A Grid-Based Bader Analysis Algorithm without Lattice Bias," *J. Phys. Condens. Matter*, **21** [8] 084204 (2009).
38. G. K. P. Dathar, W. A. Shelton, and Y. Xu, "Trends in the Catalytic Activity of Transition Metals for the Oxygen Reduction Reaction by Lithium," *J. Phys. Chem. Lett.*, **3** [7] 891-95 (2012).
39. J. W. Han and B. Yildiz, "Enhanced One Dimensional Mobility of Oxygen on Strained $LaCoO_3$(001) Surface," *J. Mater. Chem*, **21** [47] 18983-90 (2011).
40. W. Yang, Z. Wang, Z. Yang, C. Xia, R. Peng, X. Wu, and Y. Lu, "Enhanced Catalytic Activity toward O_2 Reduction on Pt-Modified $La_{1-x}Sr_xCo_{1-y}Fe_yO_{3-\delta}$ Cathode: A Combination Study of First-Principles Calculation and Experiment," *ACS Appl. Mater. Interfaces*, **6** [23] 21051-59 (2014)
41. Y. A. Mastrikov, R. Merkle, E. Heifets, E. A. Kotomin, and J. Maier, "Pathways for Oxygen Incorporation in Mixed Conducting Perovskites: A DFT-Based Mechanistic Analysis for (La, Sr)$MnO_{3-\delta}$," *J. Phys. Chem. C,* **114** [7] 3017-27 (2010).
42. Y. -L. Lee, J. Kleis, J. Rossmeisl and D. Morgan, "*Ab initio* Energetics of $LaBO_3$(001) (B = Mn, Fe, Co and Ni) for Solid Oxide Fuel Cell Cathodes," *Phys. Rev. B*, **80** [22] 224101-20 (2009).
43. Y. Xu and W. A. Shelton, "O_2 Reduction by Lithium on Au(111) and Pt(111)," *J. Chem. Phys.,* **133** [2] 024703-9 (2010).